

DESIGN OF DUAL ROTOR AXIAL FLUX PERMANENT MAGNET GENERATORS WITH FERRITE AND RARE-EARTH MAGNETS

Jawad Faiz¹, Tohid Asefi¹, Mohammad Azeem Khan²

¹School of Electrical and Computer Engineering, College of Engineering,
University of Tehran, Tehran Iran

²Department of Electrical Engineering, University of Cape Town, Cape Town, South Africa

Abstract. *This article addresses dual rotor axial flux Ferrite permanent magnet (PM) generator, as an alternative to a surface mounted and spoke types Nd-Fe-B generator which have concentrated windings. The performance parameters of all generators, particularly the efficiency, are identical. The design objective function is the generators mass minimization using a population-based algorithm. To predict the performance of the generators a finite element (FE) technique is applied. Besides, the aims of the design include minimizing cogging torque, examining different rotor pole topologies and different pole arc to pole pitch ratios. Three-dimensional FE technique is employed. It is shown that the surface mounted Ferrite generator topology cannot develop the rated torque and also has high torque ripple. In addition, it is heavier than the spoke type generator. Furthermore, it is indicated that the spoke type Ferrite PM generator has favorable performance and could be an alternative to rare-earth PM generators, particularly in wind energy applications. Finally, the performance of the designed generators is experimentally verified.*

Key words: *Axial flux, permanent magnet generator, dual rotor, finite element analysis, wind turbines, cogging torque, population-based algorithm*

1. INTRODUCTION

In recent years, permanent magnet (PM) machines have been used in different applications such as electric vehicle (EV) traction and wind energy generation. The price increase of rare-earth PMs and insecurity of their supplying are two reasons that lead to interest to substitute these PMs with alternative materials such as Ferrites. Ferrites are low cost materials to substitute rare-earth PMs [1, 2]. Some companies such as ABB have offered a Ferrite PM

Received December 26, 2019; received in revised form February 11, 2020

Corresponding author: Jawad Faiz

Electrical and Computer Engineering, College of Engineering, University of Tehran, Tehran 1439957131, Iran

E-mail: jfaiz@ut.ac.ir

*An earlier version of this paper was presented at the 14th International Conference on Applied Electromagnetics (IEEC 2019), August 26 - 28, 2019, in Niš, Serbia [1].

wind generator called the “Wind Former” [3]. In the wind former, Ferrite PMs mounted between the pole shoes of the generator. A high speed Ferrite PM motor has been introduced in [4] as a substitution to Sm-Co PMs motor. A Ferrite PM electric motor has been employed in [5] for EVs in which no-load induced phase voltage is sinusoidal and cogging torque is low [5], [6]. It is noted that the efficiency and power of the PM machines are higher than that of induction machines. This is the main reason for the substituting induction machines with PM machines [7].

A higher torque density can be obtained by axial flux PM (AFPM) machines compared to radial flux and transverse flux PM machines [8], [9]. There are two following more common radial flux PM machines:

1. Conventional radial flux (RFPM),
2. Outer rotor radial flux (ORRFPM).

and five following axial flux PM machines:

1. Double-stator axial flux (DSAFPM),
2. Double-rotor axial flux (DRAFPM),
3. Single-sided stator balanced axial flux (SBAFPM),
4. Single-sided rotor balanced axial flux (RBAFPM) and
5. Toroidal wound axial flux machines (TWAFFPM).

The advantages of the DRAFPM are the highest torque density, power density, efficiency, lowest mass of PM and active materials [10]. This motor could be the most appropriate choice in the applications requiring a high power and torque density. However, this is true specific low-power application and cannot be extended to all applications with high power and torque density.

This paper proposes a DRAFPM machine with surface mounted and spoke type Ferrite PMs which is optimally designed by a population-based algorithm. The design objective function is minimizing the mass of the machine. The 3D-FEM is used for predicting the performances of the proposed generators. The topology of the generator is determined for minimizing the cogging torque and torque ripple. The effects of pole arc/pole pitch ratio (α) upon the flux leakage, cogging torque and torque ripple are investigated by sensitivity analysis. It is noted that the air gap clearance and materials types used (except PMs) are identical. It is shown that the torque ripple, cogging torque and total harmonic distortion (THD) of the induced voltage in the spoke type ferrite PM generator at full-load are improved compared to the surface mounted Nd-Fe-B machine.

It is proved that the surface mounted Ferrite machine cannot develop the rated electromagnetic torque. Besides, it has higher torque ripple and weight compared to the spoke type machine. Therefore, the spoke type Ferrite generator can be considered as a viable alternative to the rare-earth PM generators. Finally, the performance of the designed generators is verified experimentally.

2. DIFFERENT TOPOLOGIES OF GENERATOR

Fig. 1 shows the proposed small wind generator topologies which include the spoke type and surface mounted PM rotors with laminated stator. These generators are analysed and the feasibility of substituting Nd-Fe-B PMs with Ferrite PMs in axial flux type generators is investigated.

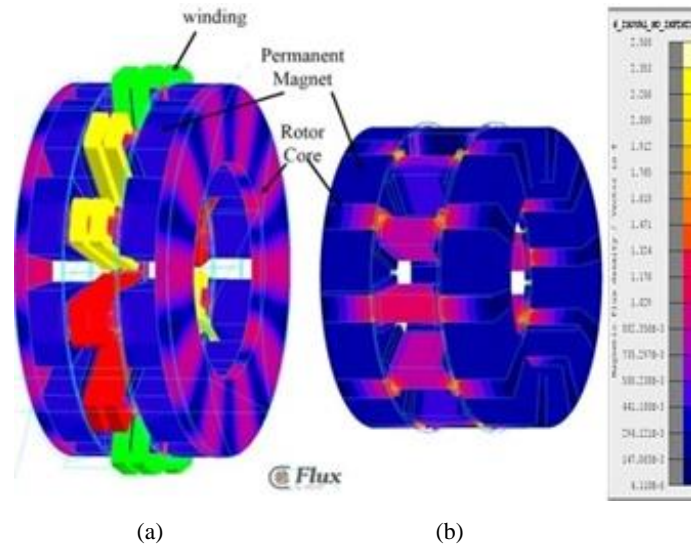


Fig. 1 Axial flux PM generator topologies (a) Ferrite surface mounted, (b) spoke type.

Fig. 2 shows the Norton magnetic equivalent circuits (MECs) of the both generators and Fig. 3 presents their flux paths. It is clear that two PMs contribute to the pole flux in the spoke type generator, whereas four PMs contribute partially to the pole flux in the surface mounted PM machine.

Performance of the designed 400 W, 10-pole, 12-slot Ferrite PM generator is compared with the corresponding surface mounted DRAFPMM having Nd-Fe-B PMs [11]. Table 1 gives the main specifications of the Nd-Fe-B generator.

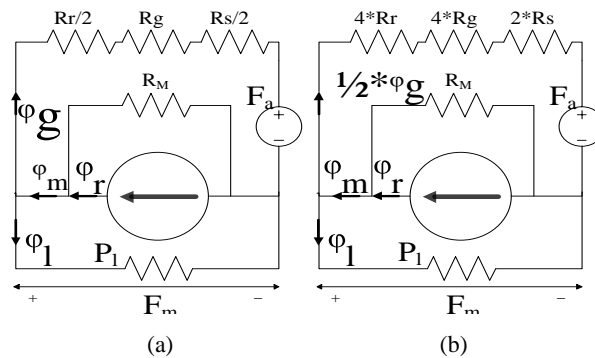


Fig. 2 MEC of PM generators (a) surface mounted and (b) spoke type.

- | | |
|---------------------------------------|---------------------------------|
| R_r : reluctance of rotor pole shoe | R_M : reluctance of PM |
| R_g : reluctance of air gap | F_a : armature reaction |
| R_s : reluctance of stator tooth | F_m : total MMF drop |
| P_l : permeance of leakage flux | C_ϕ : flux focusing factor |

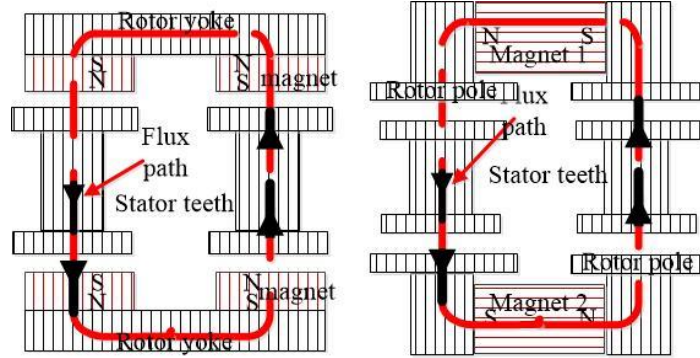


Fig. 3 Magnetic flux paths in PM Generators (a) surface mounted and (b) spoke type

Table 1 Specifications of proposed generator

Output power (W)	400
Line voltage (V)	24
Frequency (Hz)	50
Rated speed (rpm)	600
Winding type	Fractional Slot Concentrated Winding (FSCW)

For both PM arrangements, the MEC is solved and the PM surface is estimated to generate the required air gap magnetic flux B_g , for no-load spoke type machine ($F_a=0$). The coefficient f_{LKG} as the ratio of the air gap flux and magnet flux leakage is defined in [12]. Referring to Fig. 2b, as the MEC of the spoke type machines, f_{LKG} is determined as follows:

$$f_{LKG} = 0.5 \times \phi_g / \phi_M = 0.5 \times \phi_g / (0.5 \times \phi_g + \phi_L) \quad (1)$$

Fig. 3 presents the flux paths in the both machines. Generally, the leakage coefficient is less than 1 and it depends on the configuration of the machine. The FEM is applied to evaluate this coefficient in the axial flux generators design. Fig. 2b shows clearly that a fraction of total remnant magnetic flux K :

$$K = 0.25P_g / (0.25P_g + P_M + P_L) \quad (2)$$

crosses the air gap, where $P_g=1/R_g$. Therefore, the air gap magnetic flux is estimated as follows:

$$\phi_g / 2 = \frac{0.25P_g}{(0.25P_g + P_M + P_L)} \phi_r \quad (3)$$

The numerator and denominator of (3) is multiplied by the following magneto-motive force (mmf) drop:

$$mmf = F_m (2 * F_g + F_s + 2 * F_r), \quad (4)$$

and the flux is determined as follows:

$$\varphi_g / 2 = \frac{0.5 \times \varphi_g}{(0.5 \times \varphi_g + \varphi_M + \varphi_L)} \varphi_r \quad (5)$$

$$\frac{\varphi_g}{2} = \frac{0.5 \times \varphi_g / (0.5 \times \varphi_g + \varphi_L)}{(0.5 \times \varphi_g + \varphi_M + \varphi_L) / (0.5 \times \varphi_g + \varphi_L)} \times \varphi_r = \frac{f_{LKG}}{1 + f_{LKG} \times \frac{\varphi_M}{0.5 \times \varphi_g}} \times \varphi_r \quad (6)$$

$$\frac{\varphi_g}{2} = \frac{f_{LKG}}{1 + f_{LKG} \times \frac{\varphi_M}{0.5 \times \varphi_g} \times \frac{F_m}{F_m}} \times \varphi_r \quad (7)$$

$$\& \frac{F_m}{0.5 \times \varphi_g} = 4 \times R_g$$

Now by dividing the numerator and denominator of (3) to $(0.5\varphi_g + \varphi_L)$ and simplifying the resultant formula, the flux is obtained as follows:

$$\frac{\varphi_M}{F_m} = P_M \quad (8)$$

So:

$$\varphi_g / 2 = \frac{f_{LKG}}{1 + f_{LKG} \times P_M \times 4 \times R_g} \times \varphi_r \quad (9)$$

As a result, the PM surface area for generating magnetic flux φ_g in the air gap is estimated by substituting $\varphi_r = B_r A_m$ and $\varphi_g = B_g A_g$ in (9) as follows:

$$A_m = \frac{B_g}{\left(\frac{2 f_{LKG} B_r}{A_g} - \frac{4 \mu_{rec} f_{LKG} l'_g B_g}{A_g l_m} \right)} \quad (10)$$

where $l'_g = k_c l_g$, l_m is the magnet thickness and k_c is the Carter's coefficient. The same procedure is applied to the surface mounted generator and A_m is obtained as follows:

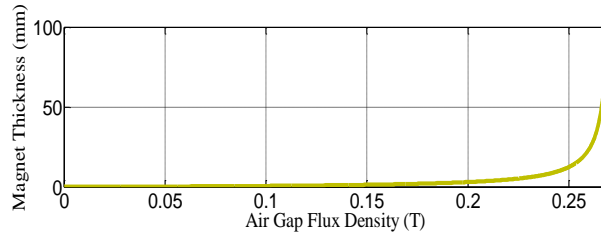


Fig. 4 Variations of air gap magnetic flux density versus PM thickness

$$A_m = \frac{B_g}{\left(\frac{f_{LKG} B_r}{A_g} - \frac{\mu_{rec} f_{LKG} l'_g B_g}{A_g l_m} \right)} \quad (11)$$

As shown in Fig 4, l_m for surface mounted Ferrite generator is calculated as follows:

$$l_m = \mu_r J_g / (B_r / B_g - 1 / (C_\phi \cdot f_{LKG})) \quad (12)$$

which indicates that l_m depends on the air gap magnetic flux density B_g . To achieve a higher power density and simplify prototyping a concentrated winding configuration is used [13].

3. DESIGN OPTIMIZATION OF DESIGNED GENERATOR

The parameters of the machines are optimized using a population-based algorithm to achieve the minimum total mass of active materials, whilst keeping the overall efficiency identical with that of the Nd-Fe-B machine. The objective function is as follows:

$$f_{new}(X) = W_{loss} \frac{f_{loss}(X)}{Loss_{min}} + W_{mass} \frac{f_{mass}(X)}{mass_{min}} \quad (13)$$

where

$Loss_{min}$ is the minimum loss,

$mass_{min}$ is the minimum mass,

$f_{Loss}(X)$ is the loss,

$f_{mass}(X)$ is the mass functions,

W_{loss} is loss weighting factor,

W_{mass} is the mass weighting factor,

as such that $W_{loss} + W_{mass} = 1$.

The same constraints are used throughout the optimization process.

The variables during the optimization process include:

1. Ratio of stator inner to outer diameter D_i/D_o ,
2. Ratio slot width to slot pitch w_s/τ_s ,
3. Air gap magnetic flux B_g ,
4. Specific electric loading A_s ,
5. Stator current density J_s ,
6. Magnet grade (residual flux density).

The f_{LKG} is determined by the FEM; considering the flux focusing factor $C_\phi = A_m/A_g$, the B_g estimated by (10), may not be increased beyond a limit as shown in Fig 4. It means that for infinite l_m , B_g of the surface mounted Ferrite generator would not exceed 0.27 T and this can be considered as a major drawback for the machine. For minimum mass of the generator, the air gap flux density is 0.24 T which is lower than that of the other topology. On the other hand, the surface mounted Ferrite generator is heavier, its axial length is longer, and its outer diameter is higher than the spoke type machine. Therefore, the surface mounted topology is less viable to replace the Nd-Fe-B machine. Table 2 and Table 3 present the optimization variables and specifications of the designed DRAFP machines. After approximately 50 generations of the optimization process, the optimum result is obtained after 50 iterations; however, the number of iterations is set up to 450 to avoid failure in a local minimum.

4. FINITE ELEMENT ANALYSIS

3D-FEM is applied to analyse the generators performance.

4.1. Magnetic flux density and back-EMF

The phase back-EMF of the DRAFPM generator can be calculated by [14]:

$$E_m = \frac{\pi}{2} f_{LKG} k_f \alpha N_{ph} k_w \omega_r D_{av} B_m L_s \quad (14)$$

where $D_{av} = (D_o + D_i) / 2$, $L_s = (D_o - D_i) / 2$ and k_f is the distribution coefficient of the air gap magnetic flux density and k_w is the winding factor

Fig. 5 and Fig. 6 presents the no-load flux density and back-EMF of the generator respectively. Table 4 gives the THD of the back-EMF for different types of PM motors.

Table 2 Optimization variables

Quantity	Variable	Min.	Max.
D_r/D_o	K_d	0.50	0.85
w_s/τ_s	---	0.50	0.70
Air-gap magnetic flux density (T)	B_g	0.20	0.75
Specific electric loading (kA/m)	A_s	9	25
Stator current density (A/mm ²)	J_s	3	8
PM grade (T)	B_r	0.30	0.41

Table 3 Specifications of proposed DRAFPM generator

Generator	Nd-Fe-B [10]	Ferrite spoke type	Surface mounted Ferrite
Magnet grade	N33-Br: 1.13T	Y33-Br: 0.41 T	
Active material (kg)	7.40	8.46	9.54
Total axial length (mm)	81.5	96	110
Outer diameter (mm)	180	170	215
Pole arc/pole pitch	0.7	0.3	0.7
Electric loading (A/m)	9885.8	10632	13557
Current density (A/mm ²)	5	5.28	5.56
Flux density of air gap B_g (T)	0.593	0.42	0.24
THD of Back EMF (%)	6.61	1.52	5.6

Table 4 THD of back-EMF of PM motors

Type of PM machine	THD of back-EMF (%)
Surface mounted Nd-Fe-B	6.61
Ferrite spoke type	1.52
Surface mounted Ferrite	5.6

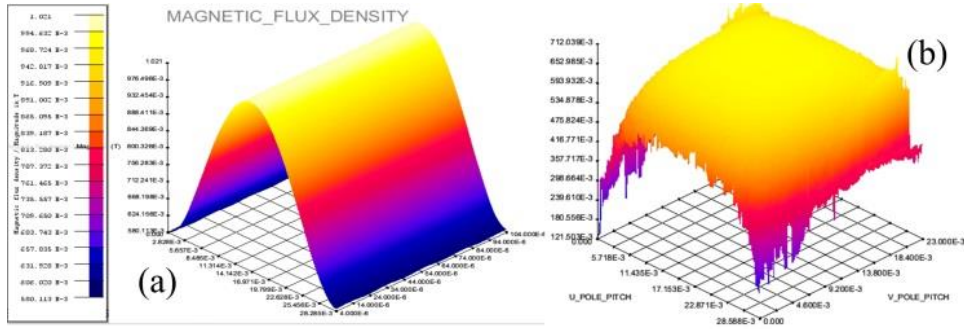


Fig. 5 No-load magnetic flux density/pole pitch of generator (a) Ferrite spoke type (b) Nd-Fe-B.

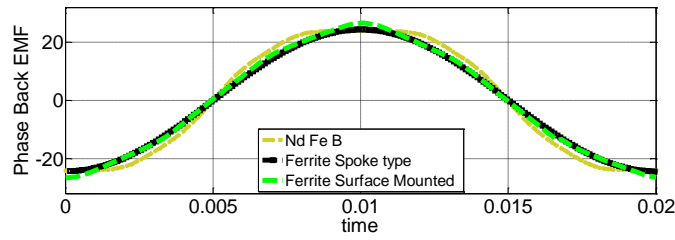


Fig. 6 Time variations of back EMF.

4.2. Full load torque and cogging torque

The cogging torque and torque component for no armature excitation case may be determined by FEM at several rotor positions and no-load condition. Fine meshes are necessary in this case.

Cogging torque is proportional to B_g^2 in the surface mounted Ferrite machine (Eq, 15). The cogging torque in this generator is small, because the air gap magnetic flux density has minimum value. However, the torque ripple is too high and it is calculated as follow [15]:

$$T_{cog}(\theta) = -\frac{\partial W(\theta)}{\partial \theta} = -\frac{\partial}{\partial \theta} \left(\frac{1}{2\mu} \int V B_g^2 dV \right) \tag{15}$$

The machine is unable to develop the rated torque. The reason is that the rotor magnetic flux excitation is weaker than that of the on-load armature reaction [10]. The developed torque is calculated as follows:

$$T = \frac{\pi^2}{4} f_{LKG} k_f \alpha k_D k_w \eta D_o^3 B_m A_m \tag{16}$$

Fig. 7 presents the developed torque and cogging torque against angular position of rotor.

4.3. Losses and efficiency

The power losses in the electric machines consist of core losses (ΔP_e), copper losses (ΔP_w) and rotational losses (ΔP_{rot}). Therefore, the total power losses of an AFPM machine is as follows:

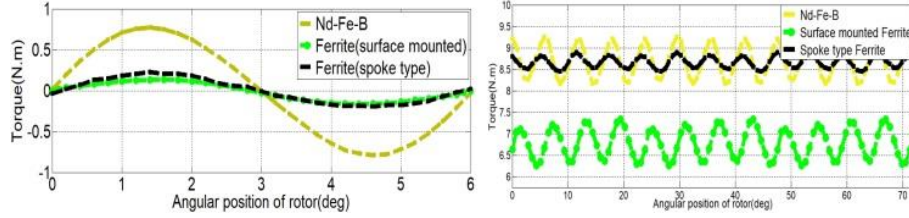


Fig. 7 Full-load torque and cogging torque of proposed generators

$$\Delta P = \Delta P_w + \Delta P_e + \Delta P_{rot} \quad (17)$$

$$\Delta P_e = \Delta P_{PM} + \Delta P_c \quad (18)$$

$$\Delta P_{rot} = \Delta P_{fr} + \Delta P_{wind} + \Delta P_{vent} \quad (19)$$

where

ΔP_{Fe} , stator core losses

ΔP_{PM} , rotor core losses

ΔP_{fr} , PM losses

ΔP_{wind} windage losses

ΔP_{ven} friction, windage and ventilation losses,

The PMs eddy current losses have a direct impact on the heat generation, the rotor temperature rise and the efficiency of the machine [16].

The resistivity of the Nd-Fe-B PM is in the range of $110-170 \times 10^{-8} \Omega m$, and the resistivity of Ferrite PMs is approximately $1000 \times 10^{-8} \Omega m$.

The Ferrite PMs is electrically insulated material and electric current does not pass it. Due to its relatively high resistance it is called Ceramic PM. Therefore, the Ferrite PM losses can be neglected for the spoke type generator [17].

Core losses in the surface mounted Ferrite generator are higher than that of the spoke type and along with higher copper losses, which decreases the overall efficiency of the generator. The generators losses components have been compared in Table 5 in which the efficiency is estimated by $P_{out} / (P_{out} + \Delta P)$.

Table 5 Comparison of performance of generators

Generator	Nd-Fe-B [9]	Spoke type ferrite	Surface mounted ferrite
Electromagnetic Torque (Nm)	8.71	8.67	6.78
Torque ripple (Nm)	1.073	0.44	1.16
Cogging Torque (Nm)	1.563	0.426	0.345
Copper losses (W)	47	51	64
Iron losses (W)	16.3	12.1	18.1
Efficiency @ 600 rpm (%)	83	82	75

4.4. Tapered pole machine

Fig. 8a presents the PM magnetic flux density distribution in a non-tapered radial sided pole machine. It is clear that the pole is partially saturated, therefore, the iron of the rotor has not been optimally used. Fig. 8b shows the tapered pole which makes possible to use iron optimally. The peak-to-peak cogging torque drops to 205 mNm, the reason is the saturation of the pole. As shown in Fig. 7, the torque ripple rises due to the non-linear behaviour of the core material; and electromagnetic torque is not developed. On the other hand, the generator active material is reduced from 8.45 kg to 7.55 kg. Fig. 9 exhibits the full load torques, and cogging torques of tapered parallel and non-tapered radial sided Ferrite generators.

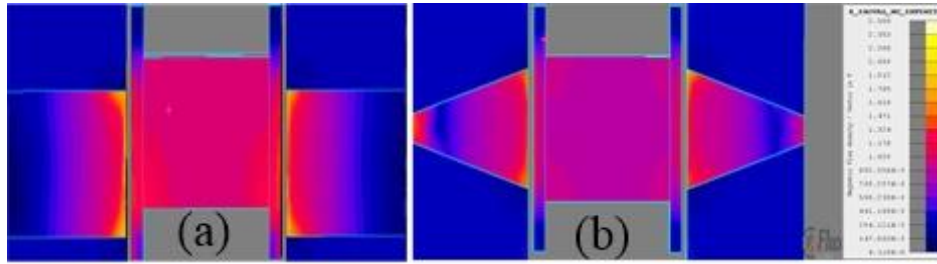


Fig. 7 (a) Flux concentration in radial sided pole and (b) tapered parallel sided pole.

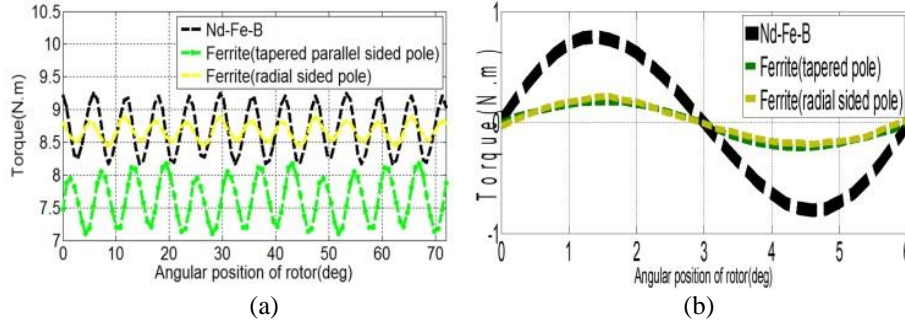


Fig. 8 (a) Full load torques, and (b) cogging torques of tapered parallel and non-tapered radial sided Ferrite generators.

4.5. Minimization of cogging torque

There are different cogging torque waveforms for various machines. These waveforms contain valuable information from the machines. The cogging torque can be estimated by quasi-3D multi-slice model as follows:

$$T_{cog}(\theta) = \frac{\pi}{3\mu_0} \sum_{s=1}^{N_c} \left[\frac{(R_{cs}^3 - R_{is}^3)}{\sum_{n=1}^{+\infty} (a_{1n}^{(III,s)} a_{4n}^{(III,s)} - a_{2n}^{(III,s)} a_{3n}^{(III,s)})} \right] \quad (20)$$

Many attempts have been made to address the cogging torque in axial flux machines [18]. However, to analyse the cogging torque of the spoke type generators, FEM is the most efficient and reliable method. A more distortion in the cogging torque generates more THD in the resultant back EMF waveform. It is evident from the resultant cogging torques shown in Fig. 10 that the smaller pole arc/pole pitch ratio leads to a more sinusoidal cogging torque waveform. Cogging torque waveforms for different pole arc/pole pitch ratios (0.3, 0.4, 0.5, 0.6 and 0.75), are investigated and ratios of 0.3 and 0.75 are shown in Fig. 9 for spoke type generator. The ratio of 0.3 has the highest peak-to-peak cogging torque and the minimum cogging torque is obtained for ratio of 0.75. Cogging torque for ratios higher than 0.75 has not been investigated, because it results in large inter-polar flux leakage, which leads to a high magnetic flux density in the rotor pole-body and improper flux distribution over the whole stator.

An air gap improper flux distribution at $\alpha=0.75$ is seen clearly from the cogging torque waveform. Also, for each value of α , PM flux leakage is calculated. Due to larger inter-polar flux leakage for higher α , flux leakages increases from 15.4% at $\alpha=0.3$ to 17.2% at $\alpha=0.75$. In Table 6, φ_{m1} and φ_{m2} is the flux through PMs contributing in the flux of one pole in spoke type generator and φ_{agap} is the air gap flux through one pole.

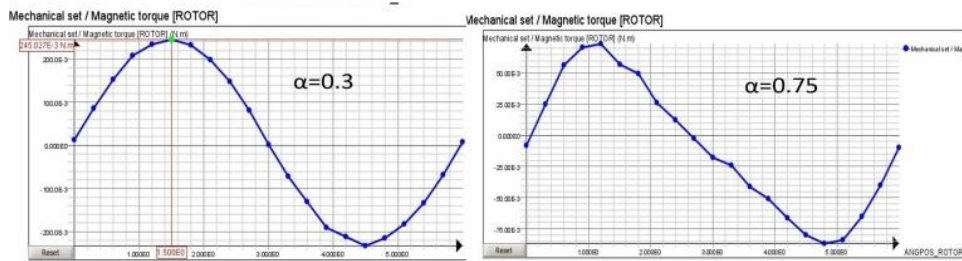


Fig. 9 Higher α increases cogging torque distortion.

Table 6 Flux leakages for different α

α	0.3	0.5	0.675	0.75
φ_{m1} (mWb)	0.2979	0.2979	0.2974	0.2969
φ_{m2} (mWb)	0.2977	0.2976	0.2980	0.2969
φ_{agap} (mWb)	0.5038	0.4967	0.4955	0.4907
φ_p (%)	15.4	16.6	16.7	17.2
f_{LKG}	0.8459	0.8341	0.8322	0.8264

5. EXPERIMENTAL VERIFICATION

It is noted that the prototyped spoke type generator is lighter than the surface mounted Ferrite generator, with lower torque ripple and able to develop the rated torque.

5.1. Structure of rotor

Fig. 10a shows the rotor of the spoke type Ferrite machine. Aluminium latches are used to retain the circumferentially magnetized magnets between the steel parts, which eliminates

the need for adhesives. To minimize vibration and noise the parts of the rotor must be carefully assembled with good tolerances.

5.2. Structure of stator

As shown in Fig. 10b, it is possible to easily and quickly wind and assemble the stator due to modular stator teeth and Aluminium. To block a path of eddy currents in the teeth of stator, only one bolt and nut is employed which keeps the laminations stacked. Fig. 10c presents the complete generator assembly. Fig. 11 exhibits the test rig of the generator. To measure the shaft torque coupled to the generator and a 3 kW servo motor, a 10 Nm torque transducer having 1% accuracy was used. A data acquisition system and a power analyser were utilized to monitor the power signals.

As shown in Fig. 12, it is necessary to analyse vibration of the heavier and more complicated rotor of spoke type Ferrite generator. Structural mechanical FE analysis was used to analyse the whole result of the test rig. To estimate the dynamics of the rotor, a modal analysis was conducted to determine the air gap unbalance.

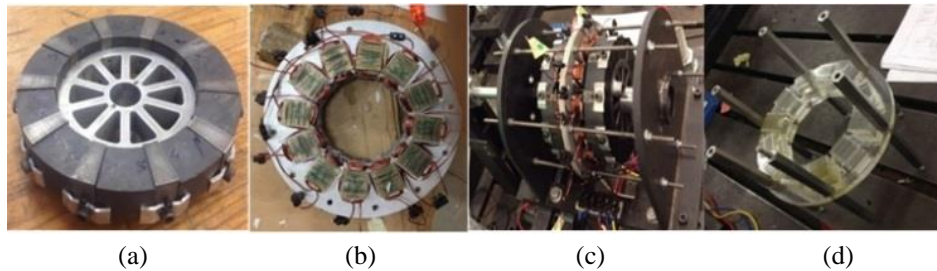


Fig. 10 (a) Rotor structure, (b) stator assembly, (c) generator assembly, and (d) dummy stator for measuring friction and windage losses.

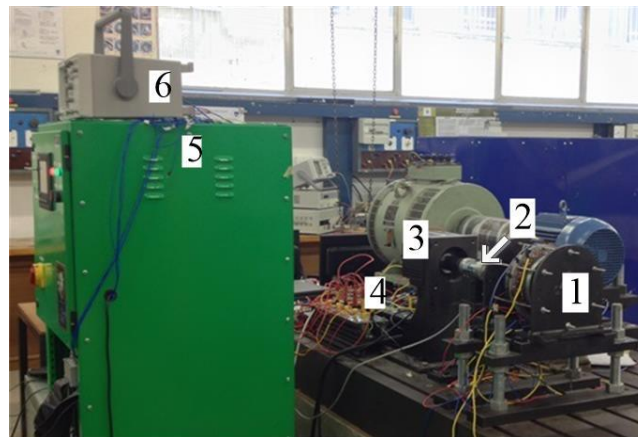


Fig. 11 Test rig: (1) generator under test, (2) 10 Nm in-line torque transducer, (3) 3 kW servo motor, (4) resistor bank, (5) servo control unit and NI cDAQ-9174 data acquisition system (6) oscilloscope.

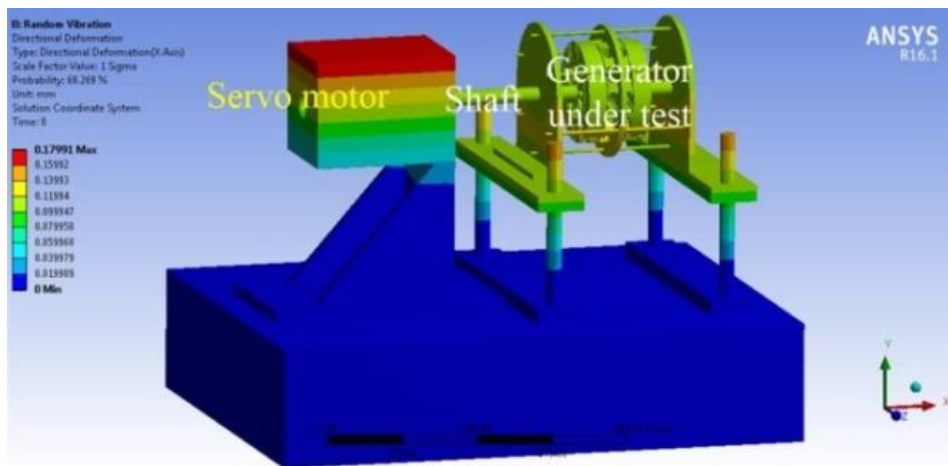


Fig. 12 Vibration analysis of whole test rig.

It was found that the total deformation of the rotor is 24 μm . The generator air gap clearance is 15 mm and the above-mentioned deformation results in a total air gap unbalance of 1.6%. As Fig. 13 shows it leads to no-load voltage unbalance. It is noted that the mechanical assembly, parts tolerances and mechanical imperfections exacerbate the unbalance in induced voltage.

5.3. Thermal behaviour of generator

The thermal behaviour of the generator is predicted in the full load and open-circuit conditions with natural air convection

Electric loading and current density of the spoke type Ferrite generator are increased 7.5 % and 5.6 % respectively compared to the proposed generator. The generator hotspot must be in the safe margin of the proposed generator's insulation class. Although a better class insulation can improve the total cost of the generator which is in contrast with the purpose of the project.

The FE technique has been chosen for thermal analysis by considering the 3D structure of the proposed generator and precise results of 3D CFD.

Although the electric loading and current density are increased, however, spoke construction of the rotor has caused the heat transfer coefficient of the surfaces in the air gap vicinity and also winding to increase which counteracts the increase of electric loading and current density and causes lower hotspot temperature in full load operation.

Fig. 14 shows the generator steady-state temperature at full load when environment temperature is 40 $^{\circ}\text{C}$. It verifies the 3D FEM results in Fig. 15, with 3 % error. This error includes error of the thermal camera image and calculations. Temperature rise in different parts of the generator has been obtained from thermal analysis and also hotspot temperature measurements of winding.

Temperature sensors in Fig. 16 shows an error of 5 % which is the error of calculations and readings from pt100 sensors.

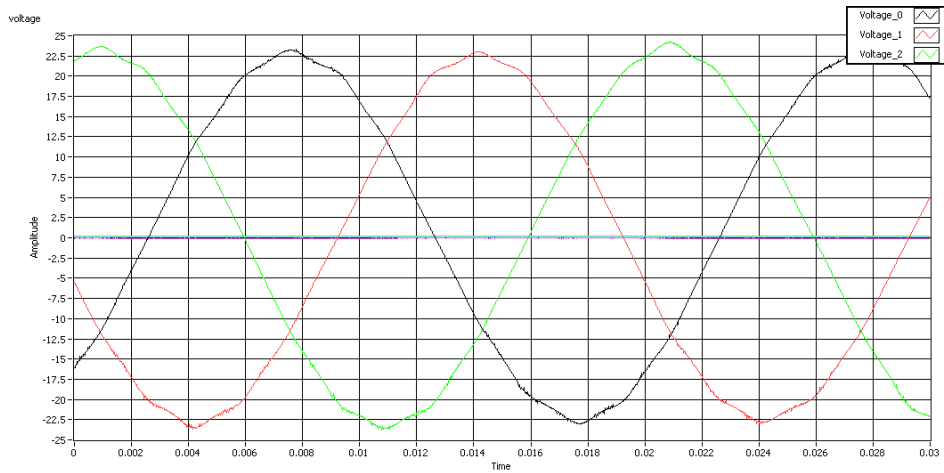


Fig. 13 Unbalance three-phase experiment no load voltages.

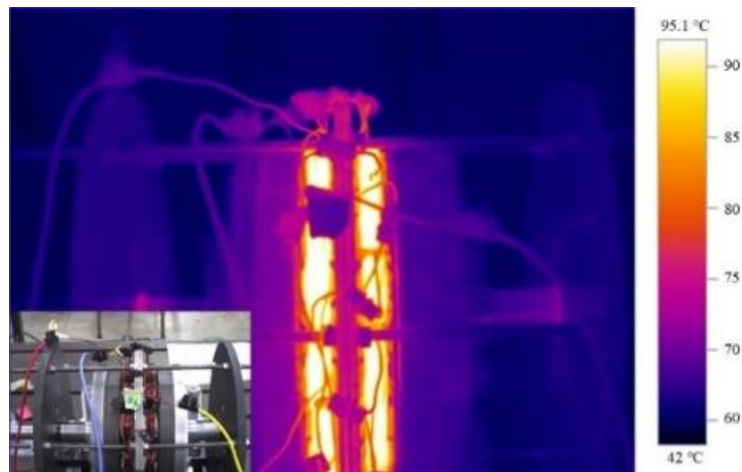


Fig. 14 Thermal image of generator at full load.

5.4. Test results

In this section the experimental results are presented and compared to the results from analytical design and numerical analysis results for the spoke type ferrite PM generator.

Fig. 17 shows the measured and numerically calculated back-emf. The total THD of the back-emf is 1.52 %. FEA of the designed generator performance agree well with the experimental results. In particular, the Dirichlet and Neumann boundary conditions were imposed, as well as precise meshing of air gap region to calculate the cogging torque.

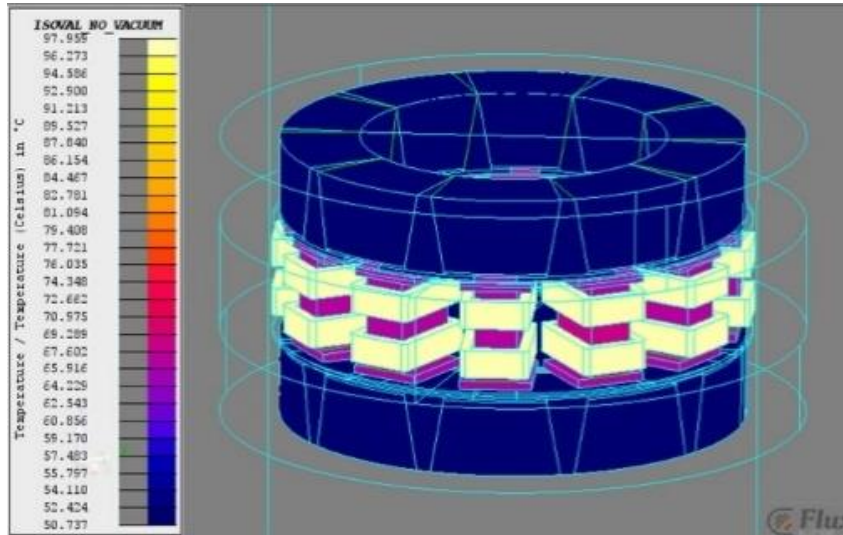


Fig. 15 Steady-state thermal analysis of generator at full load with 40 °C environment temperature.

In the no load generator, the total no load losses is measured. A dummy plastic stator of Fig. 0d was used to measure the windage and friction losses. Then, core losses are determined by deducting the windage and friction losses from the total no-load losses. To eliminate the effect of windage and friction on cogging torque, the rotor is rotated in small steps of 0.01 mechanical degrees. The torque transducer signal is then conditioned by means of a FFT and lower and higher frequencies are filtered. Fig. 18a clearly shows the generator cogging torque and its oscillations with a mechanical period of $360/LCM(2pQs) = 360/LCM(12,10) = 6^\circ$.

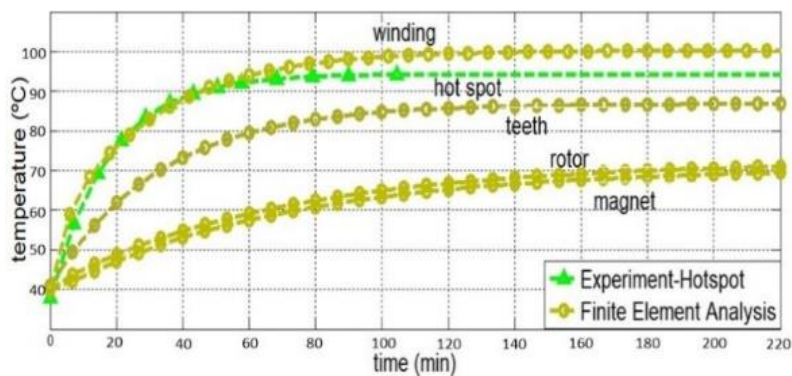


Fig. 16 Temperature rise in different parts of generator (CFD) and hotspot from pt100 sensors in windings

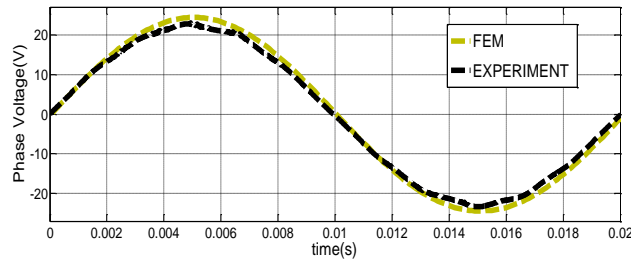


Fig. 17 Phase back EMF

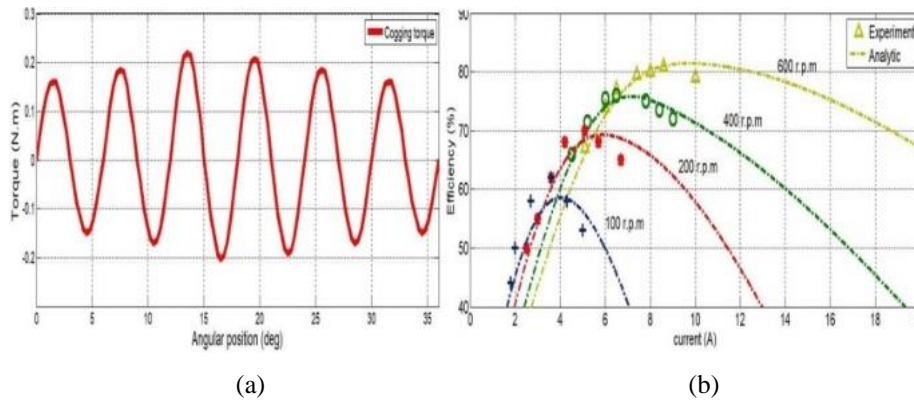


Fig. 18 (a) Cogging torque, (b) efficiency map

Table 7 Experimental results comparison of alternators at 600 rpm

Generator	Nd-Fe-B	Spoke type Ferrite
Cogging Torque (Nm)	0.52	0.23
Copper losses (W)	48	54
Iron losses (W)	19.35	15.63
Max. Efficiency (%)	80.8 @ 8.6 A	80.3 @ 8.7 A

Phase back EMF is due to asymmetries in the mechanical structure and assembly imperfections. Finally, Fig. 18b shows the efficiency map of the test machine where the measured results are compared to the analytical design. This map indicates that the maximum efficiency of the generator occurs at 87 % of the rated power, i.e. phase current of 8.7 A, at a shaft speed of 600 rpm. In Table 7 the experimental results of the Nd-Fe-B and Ferrite generators have been compared.

6. CONCLUSION

In this paper, a comparative study was conducted on the impact of the Ferrite and Nd-Fe-B magnets upon the performance of a high poles number DRAFPM wind generator. In particular, a surface mounted and spoke type topology with low cost Ferrite PMs was compared with a surface mounted Nd-Fe-B PM topology.

The designed generators were optimized to achieve minimum weight using a population-based algorithm. Extensive FEA was conducted to further optimize the machine topology with Ferrite PMs. Experimental results verified the design and FEA results. It was exhibited that the spoke type Ferrite PM topology is a viable alternative to the conventional Nd-Fe-B generator and has lower THD in its open circuit voltage, cogging torque and torque ripple. However, its active material mass was 16% more and its induced voltages were more unbalanced. It was also found that surface mounted topology is unable to develop the nominal electromagnetic torque, and also its torque ripple is higher and efficiency is lower than the spoke type generator.

REFERENCES

- [1] J. Faiz, T. Asefi and M. A. Khan, "Design of Axial Flux Ferrite Permanent Magnet Synchronous Generator", In Proceedings of the 14th International Conference on Applied Electromagnetics (IEEC 2019), August 26 - 28, 2019, Niš, Serbia.
- [2] T. Asefi, J. Faiz, and M. A. Khan. "Design of Dual Rotor Axial Flux Permanent Magnet Generators with Ferrite and Rare-Earth Magnets", In Proceedings of the IEEE 18th International Power Electronics and Motion Control Conference (PEMC), Budapest, Hungary, 2018.
- [3] M. Dahlgren, H. Frank, M. Leijon and F. Owman, "Wind Former; Wind Power Goes Large Scale," *ABB Rev.*, 3:31-37.J. , 2000.
- [4] K. H. Kim, H. I. Park, S. M. Jang, D. J. You and J. Y. Choi, "Comparative Study of Electromagnetic Performance of High-Speed Synchronous Motors With Rare-Earth and Ferrite Permanent Magnets," *IEEE Trans. Magn.*, vol. 52, no. 7, pp. 1–4, Jul. 2016.
- [5] S. Chung, S. H. Moon, D. J. Kim and J. M. Kim, "Development of a 20-Pole–24-Slot SPMSM With Consequent Pole Rotor for In-Wheel Direct Drive," *IEEE Trans. Ind. Electron.*, vol. 63, no. 1, pp. 302–309, Jan. 2016.
- [6] M. Kimiabeigi, J. D. Widmer, R. Long, Y. Gao, J. Goss, R. Martin, T. Lisle, J. M. Soler Vizan, A. Michaelides and B. Mecrow, "High-Performance Low-Cost Electric Motor for Electric Vehicles Using Ferrite Magnets," *IEEE Trans. Ind. Electron.*, vol. 63, no. 1, pp. 113–122, Jan. 2016.
- [7] I. Petrov and J. Pyrhönen, "Performance of Low-Cost Permanent Magnet Material in PM Synchronous Machines," *IEEE Trans. Ind. Electron.*, vol. 60, no. 6, pp. 2131–2138, June 2013.
- [8] Y. Chen, P. Pillay and M. Khan, "PM Wind Generator Comparison of Different Topologies," *IEEE Trans. Ind. Appl.*, vol. 41, no. 6, pp. 1619–1626, Nov. 2005.
- [9] M. A. Khan, P. Pillay and K. Visser, "On Adapting a Small PM Wind Generator for a Multi-Blade, High Solidity Wind Turbine," *IEEE Trans. Energy Convers.*, vol. 20, no. 3, pp. 685–692, Sep. 2005.
- [10] H. Jagau, M. A. Khan and P. S. Barendse, "Design of a Sustainable Wind Generator System using Redundant Materials," *IEEE Trans. Ind. Appl.*, vol. 48, no. 6, pp. 1827–1837, Nov./Dec. 2012.
- [11] J. Wanjiku, H. Jagau and M. A. Khan, "A Simple Core Structure for Small Axial-Flux PMSGs," in IEEE International Electric Machines & Drives Conference (IEMDC), Niagara Falls, May 2011.
- [12] J. R. Hendershot and T. J. E. Miller, "Design of Brushless Permanent-Magnet Motor"s, USA: Oxford University Press, 1995.
- [13] F. Gieras, R. Wang and M. J. Kamper, "Axial Flux Permanent Magnet Brushless Machines", 2nd ed, Springer, 2008.
- [14] W. Zhao, T. A. Lipo and B. Kwon, "Comparative Study on Novel Dual Stator Radial Flux and Axial Flux Permanent Magnet Motors With Ferrite Magnets for Traction Application," *IEEE Trans. Mag.*, vol. 50, no. 11, pp. 1–4, Nov. 2014.
- [15] H. Tiegna, A. Bellara, Y. Amara and G. Barakat, "Analytical Modeling of the Open-Circuit Magnetic Field in Axial Flux Permanent-Magnet Machines With Semi-Closed Slots," *IEEE Trans. on Mag.*, vol. 48, no. 3, pp. 1212–1226, Sep. 2012.
- [16] D. Ishak, Z. Q. Zhu and D. Howe, "Performance Variation of Ferrite Magnet PMSM Motor With Temperature," *IEEE Trans. Magn.*, vol. 51, no. 12, p. 95–103, Dec. 2015.
- [17] P. Zhang, G. Y. Sizov, J. He, D. M. Ionel and N. A. O. Demerdash, "Calculation of Magnet Losses in Concentrated-Winding Permanent-Magnet Synchronous Machines Using a Computationally Efficient Finite-Element Method," *IEEE Trans. Ind. Appl.*, vol. 49, no. 6, pp. 1495–1504, Nov./Dec. 2013.
- [18] J. G. Wanjiku, M. Khan, P. Barendse and P. Pillay, "Influence of Slot Openings and Tooth Profile on Cogging Torque in Axial-Flux PM Machines," *IEEE Trans. Ind. Electron.*, vol. 62, no. 12, pp. 7578–7589, Dec. 2015.